LETTERS
PUBLISHED ONLINE: 22 FEBRUARY 2016 | DOI: 10.1038/NNANO.2016.3
nature nanotechnology

Chiral atomically thin films

Cheol-Joo Kim[1], A. Sánchez-Castillo[2], Zack Ziegler[1], Yui Ogawa[1,3], Cecilia Noguez[4] and Jiwoong Park[1,5]*

Chiral materials possess left- and right-handed counterparts linked by mirror symmetry. These materials are useful for advanced applications in polarization optics[1,2], stereochemistry[3,4] and spintronics[5,6]. In particular, the realization of spatially uniform chiral films with atomic-scale control of their handedness could provide a powerful means for developing nanodevices with novel chiral properties. However, previous approaches based on natural or grown films[1,2,7,8], or arrays of fabricated building blocks[9–11], could not offer a direct means to program intrinsic chiral properties of the film on the atomic scale. Here, we report a chiral stacking approach, where two-dimensional materials are positioned layer-by-layer with precise control of the interlayer rotation (θ) and polarity, resulting in tunable chiral properties of the final stack. Using this method, we produce left- and right-handed bilayer graphene, that is, a two-atom-thick chiral film. The film displays one of the highest intrinsic ellipticity values (6.5 deg μm^{-1}) ever reported, and a remarkably strong circular dichroism (CD) with the peak energy and sign tuned by θ and polarity. We show that these chiral properties originate from the large in-plane magnetic moment associated with the interlayer optical transition. Furthermore, we show that we can program the chiral properties of atomically thin films layer-by-layer by producing three-layer graphene films with structurally controlled CD spectra.

Our approach for generating chiral twisted bilayer graphene with precisely controlled interlayer structures (θ and rotational polarity) relies on two key steps (Fig. 1a): first, a single-layer graphene film is grown with a uniform crystalline orientation over the entire film; second, this film is cut into multiple pieces and is stacked layer-by-layer with a controlled θ_{stack} on the basis of the known crystalline orientation while rotating anticlockwise or clockwise to form left- or right-handed films that are connected by a mirror plane (vertical dashed line), respectively. Using our method, we generate chiral twisted bilayer graphene films, where their θ and handedness are controlled uniformly over several millimetres with a high yield of interlayer coupling[12–14] (see Methods and Supplementary Figs 1–4 for more details). Figure 1b shows the electronic band structures (top images) and the cross-sectional schematics (bottom images) of left- and right-handed twisted bilayer graphene with spiral atomic arrangements of opposite handedness. Regardless of the handedness, the electronic band structure and the electrical and optical properties of twisted bilayer graphene can be tuned using θ (refs 15,16), as the electronic states from each layer hybridize near degeneracy, producing interlayer optical absorption resonance whose peak energies (denoted E_A and E_B, inset of Fig. 2a) are continuously tunable over a broad optical bandwidth. However, the intrinsic chiral properties of bilayer graphene have not been reported[17].

These bilayer films show strong CD and absorb left and right circularly polarized light by different amounts, as shown in Fig. 1c, where we plot the ellipticity (Ψ) spectra (or CD spectra), measured from the left-handed (red) and right-handed (blue) twisted bilayer graphene samples with $\theta_{stack} = 16.5°$, and single-layer graphene (grey), shown for comparison. Here, Ψ characterizes the polarization change of the light transmitting perpendicularly through the films (upper schematic, Fig. 1c), and is proportional to the absorption difference between the left and right circularly polarized light (I_L and I_R) according to the relationship, $\Psi = (I_L - I_R)/2(I_L + I_R)$. Unlike the CD spectra of single-layer graphene, which show negligible values over the entire measurement photon energy range, the CD spectra of left- and right-handed twisted bilayer graphene each show two strong peaks, one with a positive sign and the other with a negative sign, regardless of the in-plane sample orientation (see Supplementary Fig. 5). Significantly, Ψ measured from twisted bilayer graphene flips its sign depending on the handedness of the twisted bilayer graphene, whereas the two CD peak energies are similar to those of the interlayer transitions ($E_A = 2.8$ eV and $E_B = 4.6$ eV, for $\theta = 16.5°$), suggesting the direct correlation between the CD spectra and the structure of twisted bilayer graphene (θ and handedness).

The magnitude of the CD peak we observe is as large as 4.3 mdeg (Fig. 2a), a remarkably large value given the two-atom thickness of our twisted bilayer graphene films ($t_{BL} = 0.66$ nm). In comparison, a much thicker film would be needed to generate a CD peak of similar magnitude in other natural chiral molecules. (for example, 50 nm for D-glucose, 100 μm for camphorsulfonic acid)[7,18] (see Supplementary Table 1). Indeed, the ellipticity normalized to the film thickness, a material-specific parameter, is as large as 6.5 deg μm^{-1} in our chiral twisted bilayer graphene ($\theta = 24.5°$, Fig. 2a), one of the highest intrinsic values ever reported.

This large CD behaviour is observed in all of our twisted bilayer graphene films. Moreover, their CD peak energy and sign can be directly tuned using θ and the rotational polarity of the stacked layer. Figure 2a presents data from six chiral pairs of twisted bilayer graphene (black: left-handed, grey: right-handed) with different θ. It can be seen that every CD spectra has two peaks, one at lower energy (Peak A) and the other at higher energy (Peak B), each closely matching the interlayer resonance energy, E_A (marked by a triangle) or E_B (a diamond)[14]. In addition, the two peaks in each CD spectra have opposite sign, whereas the entire spectrum changes its sign (but not shape) for the opposite handedness of twisted bilayer graphene with the same θ. Figure 2b further shows a three-dimensional colour plot of Ψ (red: positive, blue: negative) from 29 twisted bilayer graphene samples. The most striking feature in Fig. 2b is the two lines (denoted $\sigma+$ and $\sigma-$), along which all CD peaks are found. Along the $\sigma+$ line, we find strongly positive Ψ, corresponding to Peak A

[1]Department of Chemistry and Chemical Biology, Cornell University, Ithaca, New York 14853, USA. [2]Escuela Superior de Apan, Universidad Autónoma del Estado de Hidalgo, Chimalpa Tlalayote, Municipio de Apan, Hidalgo 43920, México. [3]Institute for Materials Chemistry and Engineering, Kyushu University, Kasuga, Fukuoka 816-8580, Japan. [4]Instituto de Física, Universidad Nacional Autónoma de México, Apartado Postal 20-364, México D.F. 01000, México. [5]Kavli Institute at Cornell for Nanoscale Science, Cornell University, Ithaca, New York 14853, USA. *e-mail: jpark@cornell.edu

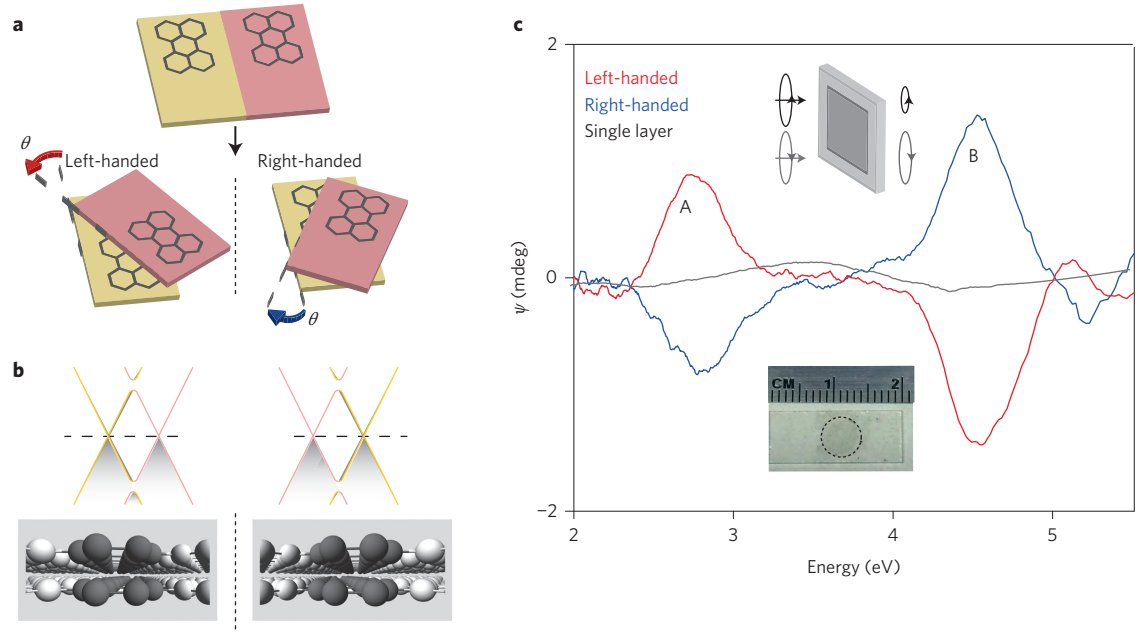

Figure 1 | Chiral atomically thin films produced by chiral stacking. a, Schematic of the chiral stacking process for generating left- and right-handed twisted bilayer graphene films connected by a mirror plane (vertical line). **b**, Electronic band structures (top images) and cross-sectional schematics with spiral atomic arrangements (bottom images) of left- and right-handed twisted bilayer graphene films. **c**, Ellipticity (Ψ) spectra, or circular dichroism (CD) spectra, measured from a pair of chiral twisted bilayer graphene films with $\theta = 16.5°$ (red: left-handed, blue: right-handed) and single-layer graphene (grey). The CD spectra of left- and right handed-twisted bilayer graphene each show two strong peaks, denoted Peak A and B. Lower inset: Photograph of a twisted bilayer graphene film (circled area; 5 mm in diameter) on a fused silica substrate. Upper inset: Schematic for Ψ measurements, where twisted bilayer graphene absorbs left- and right-handed circularly polarized light differently.

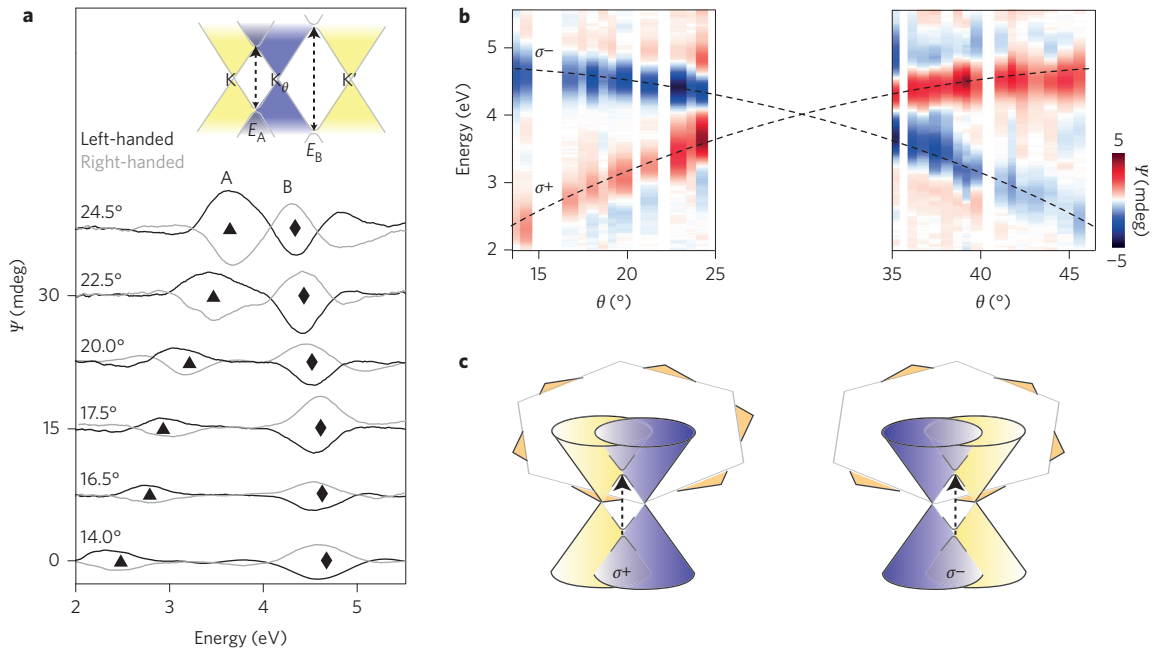

Figure 2 | Programming CD spectra in twisted bilayer graphene with θ dependent interlayer optical transitions. a, CD spectra in chiral twisted bilayer graphene pairs with different θ. The spectra are offset by 7.5 mdeg for clarity. Inset: Band structure of twisted bilayer graphene, where the K (or K′) Dirac cone of the bottom layer (yellow) is hybridized with the K_θ Dirac cone of the top layer (blue) producing the interlayer optical transition E_A (or E_B). The energy of E_A (E_B) is marked by a triangle (diamond) in the spectra. **b**, Three-dimensional CD plot as a function of θ (x axis) and energy of incident light (y axis), taken from 29 twisted bilayer graphene samples in total. Here, the results from right-handed samples with θ is plotted at $60°–\theta$ (box on the right side) instead of $-\theta$, as they are equivalent because of the six-fold rotational symmetry of the graphene lattice. All CD peaks are found along two lines (σ+: positive Ψ, σ−: negative Ψ), which indicate the energies of interlayer optical transitions. **c**, For each interlayer optical transition, the top-layer Dirac cone (blue) can be rotated with respect to that of the bottom layer (yellow) either anticlockwise (left; corresponding to σ+) or clockwise (right; σ−), which determines the sign of the CD signal.

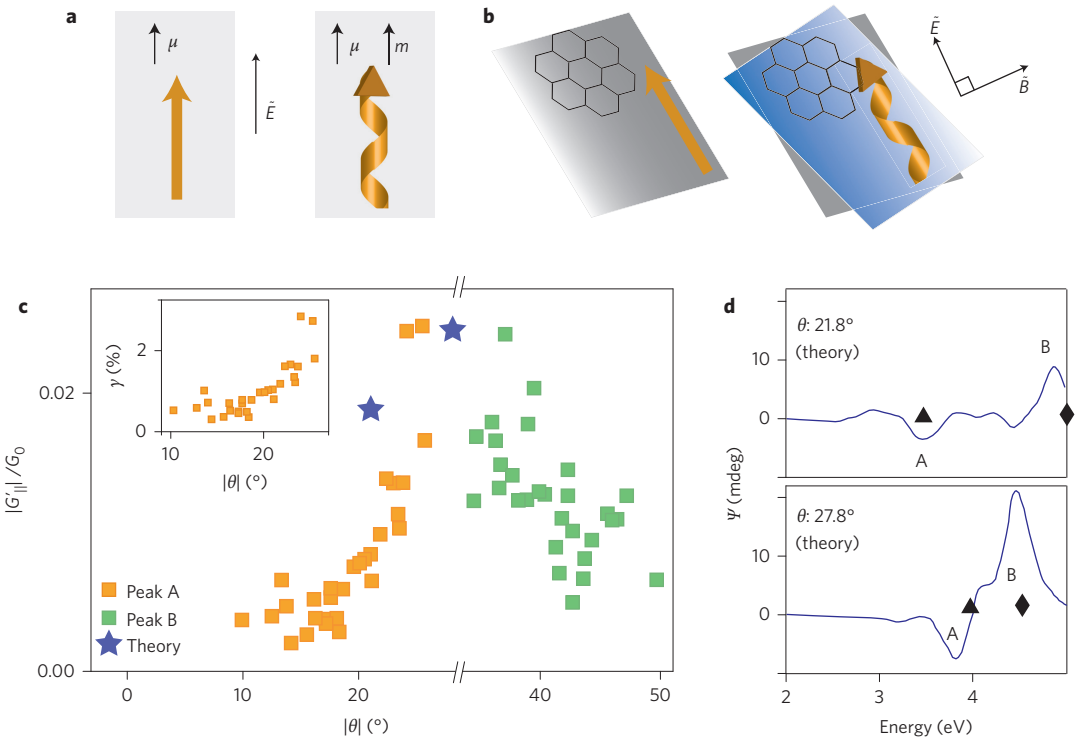

Figure 3 | In-plane magnetic moment as the origin of the CD in twisted bilayer graphene. a, When light with oscillating electric field ($\tilde{E}$) induces dynamic current (orange arrows), an electric dipole μ is excited both in achiral (left panel) and chiral (right panel) materials. In chiral materials, a magnetic moment m, whose orientation changes with the structural chirality, is also excited (right panel). **b**, Interlayer optical transitions in twisted bilayer graphene generate excited states delocalized across both layers, which can host a helical current with an in-plane magnetic moment (right panel), unlike in single-layer graphene (left panel). **c**, Plot of peak $|G'_{\|}|$, the coupled electric-magnetic dipole polarizability in twisted bilayer graphene as a function of $|\theta|$ (in units of $G_0 = e^2/4\hbar$). It includes experimental results from Peak A (orange square) and Peak B (green square), as well as the calculated values (blue star). Inset: Plot of $\gamma = |G'_{\|}|/\sigma_{\text{inter},\|}$, which provides a measure of the chiral portion of the interlayer transition ($\sigma_{\text{inter},\|}$). **d**, Theoretical Ψ spectra of right-handed twisted bilayer graphene with θ of 21.8° and 27.8°, generated based on our first-principles calculations. The triangles (diamonds) denote the calculated interlayer transition energies, E_A (E_B).

of the left-handed film or Peak B of the right-handed film. Along the $\sigma-$ line, conversely, strongly negative Ψ is observed, including both Peak B of the left-handed film and Peak A of the right-handed film. Significantly, the peak energy–θ relation closely follows that of the interlayer optical transition (dotted lines) previously studied by both experiments and theory based on a tight-binding model[14,19].

These observations confirm that the θ-dependent interlayer optical transition is responsible for the large CD in chiral twisted bilayer graphene. In addition, the sign of Ψ is directly correlated with the sense of rotation between the two Dirac cones associated with the specific interlayer optical transition, as depicted in Fig. 2c. Specifically, the Dirac cone from the top layer (blue) is rotated with respect to that of the bottom layer (yellow) either anti-clockwise (left, Fig. 2c; corresponding to $\sigma+$), or clockwise (right, Fig. 2c; $\sigma-$). This feature is consistent with the CD sign change according to the structural handedness of twisted bilayer graphene, and it also explains the opposite signs of Peak A and Peak B within the same twisted bilayer graphene, as the hybridized electronic states for E_A and E_B (inset, Fig. 2a) involve complementary pairs of Dirac cones with the opposite rotational polarity (for example, clockwise θ versus anticlockwise 60°-θ). The direct correlation between the peak energy and polarity of Ψ and the electronic band structure proves that the chiroptical effects are indeed intrinsic electronic CD, different from other effects induced by surface impurities or buckled structures[20,21].

The CD in twisted bilayer graphene originates from the chiral in-plane magnetic dipole moment associated with the interlayer optical transition[22], as described in Fig. 3a. When light (oscillating electric field, $\tilde{E}$) excites an electric dipole (μ), this generates a dynamic current, thereby producing optical absorption in both achiral (left) and chiral (right) materials. In chiral materials, a magnetic dipole moment (m), which is associated with a solenoid-like helical current, can also be generated simultaneously. As a result, m will disappear in single-layer graphene or for intralayer absorption in twisted bilayer graphene as the excited states localized within one layer cannot form a helical current circling out-of-plane (left image, Fig. 3b). On the other hand, an interlayer optical transition in twisted bilayer graphene excites a hybridized state delocalized across both layers, which can host a helical current (right image, Fig. 3b) with m. In general, the magnitude of this induced magnetic moment is determined by the coupled electric–magnetic dipole polarizability ($G = G' + iG''$; unit: Ω^{-1}) following $m = G\tilde{E}$, and the interaction between the light magnetic field and m generates an additional chiral optical absorption term ($\pm k|E|^2G'$; where k is the light wavevector), whose sign changes with the structural chirality (the sign of G') and the circular polarization of light ($\pm$).

Quantitatively, the ellipticity value in twisted bilayer graphene is given by $\Psi = (kt_{\text{BL}})(G'_{\|}/\sigma_{\|})$, where $G'_{\|}$ and $\sigma_{\|}$ are the multipole sheet polarizability and the optical sheet conductivity of twisted bilayer graphene (ranging between $2G_0$ and $8G_0$, where $G_0 = e^2/4\hbar$) perpendicular to the propagating light, respectively (see first-principles calculation of ψ in the Supplementary Information). The ellipticity has two unitless parts: kt_{BL} (0.01 at 3 eV), a wavelength-dependent geometric factor, and the ratio between $G'_{\|}$ and $\sigma_{\|}$, which may be interpreted as the portion of the chiral (or helical) dynamic current generated by light. Therefore, the experimental values of

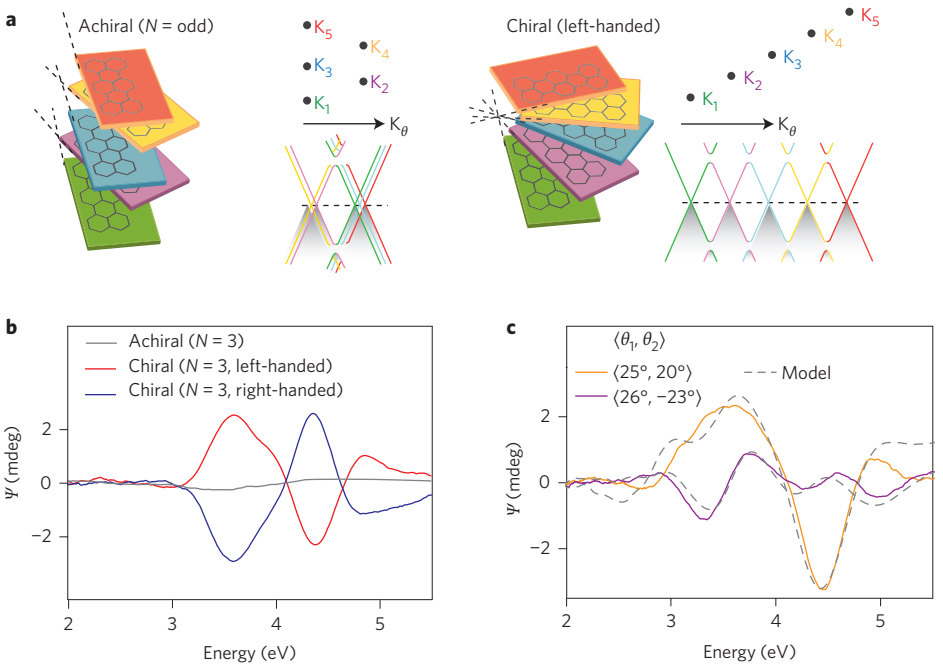

Figure 4 | Programming CD spectra in multilayer graphene films. a, Schematics of achiral (left) and chiral (right) multilayer graphene and their respective band structures. With a single value of $|\theta|$ for each stacking, an achiral (or chiral) structure can be fabricated by alternating θ and $-\theta$ (or by repeating the same θ). K_n represents the position of the Dirac point of nth single-layer graphene in the momentum space. **b**, CD spectra measured from two chiral twisted trilayer graphene films (red: left-handed, blue: right-handed) and an achiral twisted trilayer graphene film (grey), all fabricated with $|\theta| = 25°$. **c**, Programming Ψ spectra of twisted trilayer graphene with $|\theta_1| \neq |\theta_2|$, where θ_1 (θ_2) is the angle between bottom and middle (middle and top) layers. The solid orange (purple) line presents the measured spectra of twisted bilayer graphene with $\langle 25°, 20° \rangle$ ($\langle 26°, -23° \rangle$) and the dotted grey lines plot predicted values generated by simply adding the two previously measured CD spectra of twisted bilayer graphene with θ_1 and θ_2, shown in Fig. 2.

Ψ and $\sigma_{\|}$ allow us to directly measure $G'_{\|}$ and to estimate the chiral portion of the interlayer absorption that produces the CD. Figure 3c (main panel) plots $|G'_{\|}|/G_0$ as a function of θ based on our data and shows a rapid increase of $|G'_{\|}|$ as θ approaches 30° with a consistently large value over 0.01 G_0 for $20° < \theta < 40°$. In addition, the inset of Fig. 3c plots the ratio $\gamma = |G'_{\|}|/\sigma_{\mathrm{inter},\|}$ and shows values as large as 2.8%. This explains that a significant portion of the interlayer transition (corresponding to $\sigma_{\mathrm{inter},\|}$) is chiral, producing the large CD we observed.

Our first-principles calculation based on density-functional theory confirms that the large coupled polarizability G originates from the CD in twisted bilayer graphene. We conducted first-principles calculations of both G and absorption in twisted bilayer graphene after full structural relaxation, and then generated the Ψ spectra on the basis of this[23–29] (see calculation of ψ in the Supplementary Information). Figure 3d presents the calculated Ψ spectra for right-handed twisted bilayer graphene with θ of 21.8° and 27.8°. Notably, Peak A with negative sign and Peak B with positive sign are reproduced in both cases, whereas Ψ remains small elsewhere. Their peak energies are consistent with the calculated interlayer transition energies, E_A (triangle) and E_B (diamond), confirming that the interlayer absorption is essential for large Ψ (Supplementary Fig. 6). The calculated values of $|G'_{\|}|$ (blue stars) are close to the experimental values, as shown in Fig. 3c. Furthermore, the calculated ellipticities of Peak A (3.5 mdeg for 21.8° and 4.6 mdeg for 27.8°) are in good agreement with the experimental values observed from our samples with similar angles (2 mdeg for 21.8° and 4.1 mdeg for 25.3°). The calculated magnitudes for Peak B (8.5 and 20 mdeg, respectively) are larger than the experimental values (2.4 and 2.9 mdeg), a discrepancy we ascribe to many-body excitonic effects that become more pronounced at higher energies[14] (these effects have not been included in our calculations).

More generally, our chiral stacking method allows us to design chiral multilayer graphene films (N layers) with unique chiral properties by individually programming θ_1, θ_2, …, θ_{N-1}. Even with a single value of $|\theta|$, one can create many different variations of multilayer graphene films with different symmetries. For instance, alternating θ and $-\theta$ would result in an achiral multilayer graphene with an overall band structure similar to that of a single twisted bilayer graphene structure (left image, Fig. 4a), as it has a vertical mirror symmetry when N is odd. Conversely, repeating θ for each transfer would create a completely chiral multilayer graphene (right image, Fig. 4a) with its electronic band structure producing periodic band extrema and crossings at multiple points in the momentum space.

In Fig. 4b,c, we demonstrate this capability by producing twisted trilayer graphene with different symmetries and CD spectra. Figure 4b presents the CD spectra measured from three different twisted trilayer graphene films, in all of which θ_1 and θ_2 are close to 25°. Two of them have a periodic helical structures (red: left-handed, blue: right-handed) and show enhanced CD peaks. In these helical films, each-single-layer graphene film is rotated relative to the others with the same polarity, and changing the rotational direction reverses the overall handedness, producing CD spectra with the opposite sign. For the non-helical film (grey curve), where θ_1 and θ_2 have the opposite polarity, the CD signal is negligible, as it now has a mirror symmetry around the middle layer. More generally, our approach allows one to program the shapes of the CD spectra by controlling θ_1 and θ_2 of twisted trilayer graphene independently. In Fig. 4c, the CD spectra measured from twisted trilayer graphene for $\langle \theta_1, \theta_2 \rangle = \langle 25°, 20° \rangle$ and $\langle 26°, -23° \rangle$ closely match the predicted ones (dotted lines) calculated by simply adding the two CD spectra of twisted bilayer graphene with θ_1 and θ_2 that we measured previously (shown in Fig. 2), demonstrating the general fidelity of our process for designing CD in multilayer samples.

Our fabrication process and tunable chiral properties can be extended from graphene to other two-dimensional layered materials to form chiral atomically thin films[17]. This would allow the realization of chiral properties with diverse electrical and optical features (such as absorption-based CD versus circular birefringence; see Supplementary Fig. 7) and the investigation of the coupling between the structural chirality and the spin and valley degrees of freedom[30]. Ultimately, our chiral stacking approach together with a fundamental understanding of the material's chirality dependent properties could enable the production of multi-functional integrated circuits based on ultrathin devices with advanced electrical, optoelectronic, spintronic and chemical sensing functionalities.

Methods

Methods and any associated references are available in the online version of the paper.

Received 11 September 2015; accepted 7 January 2016; published online 22 February 2016

References

1. Tang, Y. & Cohen, A. E. Optical chirality and its interaction with matter. *Phys. Rev. Lett.* **104,** 163901 (2010).
2. Barron, L. D. *Molecular Light Scattering and Optical Activity* (Cambridge Univ. Press, 2009).
3. Smith, M. B. & March, J. *March's Advanced Organic Chemistry: Reactions, Mechanisms and Structure* (Wiley, 2007).
4. Inoue, Y. & Ramamurthy, V. *Chiral Photochemistry* (Marcel Dekker, 2004).
5. Göhler, B. *et al.* Spin selectivity in electron transmission through self-assembled monolayers of double-stranded DNA. *Science* **331,** 894–897 (2011).
6. Koehl, W. F. *et al.* Current-induced spin polarization in gallium nitride. *Appl. Phys. Lett.* **95,** 072110 (2009).
7. Matsuo, K. & Gekko, K. Vacuum-ultraviolet circular dichroism study of saccharides by synchrotron radiation spectrophotometry. *Carbohydr. Res.* **339,** 591–597 (2004).
8. Verbiest, T. *et al.* Strong enhancement of nonlinear optical properties through supramolecular chirality. *Science* **282,** 913–915 (1998).
9. Kuwata-Gonokami, M. *et al.* Giant optical activity in quasi-two-dimensional planar nanostructures. *Phys. Rev. Lett.* **95,** 227401 (2005).
10. Gibbs, J. G., Mark, A. G., Eslami, S. & Fischer, P. Plasmonic nanohelix metamaterials with tailorable giant circular dichroism. *Appl. Phys. Lett.* **103,** 213101 (2013).
11. Shopsowitz, K. E., Qi, H., Hamad, W. Y. & Maclachlan, M. J. Free-standing mesoporous silica films with tunable chiral nematic structures. *Nature* **468,** 422–425 (2010).
12. Brown, L. *et al.* Polycrystalline graphene with single crystalline electronic structure. *Nano Lett.* **14,** 5706–5711 (2014).
13. Havener, R. W. *et al.* Hyperspectral imaging of structure and composition in atomically thin heterostructures. *Nano Lett.* **13,** 3942–3946 (2013).
14. Havener, R. W., Liang, Y., Brown, L., Yang, L. & Park, J. Van Hove singularities and excitonic effects in the optical conductivity of twisted bilayer graphene. *Nano Lett.* **14,** 3353–3357 (2014).
15. Lopes dos Santos, J. M. B., Peres, N. M. R. & Castro Neto, A. H. Graphene bilayer with a twist: electronic structure. *Phys. Rev. Lett.* **99,** 256802 (2007).
16. Li, G. *et al.* Observation of Van Hove singularities in twisted graphene layers. *Nature Phys.* **6,** 109–113 (2010).
17. Geim, A. K. & Grigorieva, I. V. Van der Waals heterostructures. *Nature* **499,** 419–425 (2013).
18. Stein, G., Stein, J. & Kleinsmith, L. J. (eds) *Methods in Cell Biology* Vol. 18 (Academic, 1978).
19. Moon, P. & Koshino, M. Optical absorption in twisted bilayer graphene. *Phys. Rev. B* **87,** 205404 (2013).
20. Lehtinen, P. O. *et al.* Magnetic properties and diffusion of adatoms on a graphene sheet. *Phys. Rev. Lett.* **91,** 017202 (2003).
21. Levy, N. *et al.* Strain-induced pseudo-magnetic fields greater than 300 Tesla in graphene nanobubbles. *Science* **329,** 544–547 (2010).
22. Yang, N. & Cohen, A. E. Local geometry of electromagnetic fields and its role in molecular multipole transitions. *J. Phys. Chem. B* **115,** 5304–5311 (2011).
23. Sánchez-Castillo, A. & Noguez, C. Understanding optical activity in single-walled carbon nanotubes from first-principles studies. *J. Phys. Chem. C* **114,** 9640–9644 (2010).
24. Hidalgo, F., Sánchez-Castillo, A. & Noguez, C. Efficient first-principles method for calculating the circular dichroism of nanostructures. *Phys. Rev. B* **79,** 075438 (2009).
25. Noguez, C. & Hidalgo, F. *Ab initio* electronic circular dichroism of fullerenes, single-walled carbon nanotubes, and ligand-protected metal nanoparticles. *Chirality* **26,** 553–562 (2014).
26. Soler, J. M. *et al.* The SIESTA method for *ab initio* order-*N* materials simulation. *J. Phys. Condens. Matter* **14,** 2745–2779 (2002).
27. Troullier, N. & Martins, J. L. Efficient pseudopotentials for plane-wave calculations. *Phys. Rev. B* **43,** 1993–2006 (1991).
28. Perdew, J. P. & Zunger, A. Self-interaction correction to density-functional approximations for many-electron systems. *Phys. Rev. B* **23,** 5048–5079 (1981).
29. Perdew, J. P., Burke, K. & Ernzerhof, M. Generalized gradient approximation made simple. *Phys. Rev. Lett.* **77,** 3865–3868 (1996).
30. Xu, X., Yao, W., Xiao, D. & Heinz, T. F. Spin and pseudospins in layered transition metal dichalcogenides. *Nature Phys.* **10,** 343–350 (2014).

Acknowledgements

We thank P.L. McEuen, F. Wang, K.F. Mak and M.W. Graham for useful discussions and M.P. Levendorf for experimental help. This work was supported by the National Science Foundation (NSF) through the Cornell Center for Materials Research (NSF DMR-1120296), the AFOSR (FA2386-13-1-4118), and the Nano Material Technology Development Program through the National Research Foundation of Korea (NRF) funded by the Ministry of Science, ICT, and Future Planning (2012M3A7B4049887). Y. Ogawa was partially supported by Grant-in-Aid for JAPS Fellows. A. Sánchez-Castillo and C. Noguez were supported by DGAPA-UNAM (PAPIIT IN107615) and CONACyT (179454). Sample fabrication was performed at the Cornell Nanoscale Science & Technology Facility, a member of the National Nanotechnology Infrastructure Network, which is supported by the National Science Foundation (ECS-0335765).

Author contributions

C.-J.K. and J.P. designed the experiments. C.-J.K. and Y.O. grew graphene samples. C.-J.K. and Z.Z. conducted the sample fabrication and optical characterization. A.S.-C. and C.N. performed the first-principles calculation of CD effects. C.-J.K. and J.P. carried out data analysis and wrote the manuscript with input from all authors.

Additional information

Supplementary information is available in the online version of the paper. Reprints and permissions information is available online at www.nature.com/reprints. Correspondence and requests for materials should be addressed to J.P.

Competing financial interests

The authors declare no competing financial interests.

Methods

Aligned graphene growth. To grow graphene with an aligned crystalline orientation, we conduct chemical vapour deposition on a recrystallized copper (111) surface using a recipe slightly modified from that reported in our previous study[12]. The detailed procedure is described below:

(1) Load a copper foil (Nilaco Corporation, #CU-113213, 99.9% purity) in a hot wall, vacuum furnace.
(2) Ramp up the temperature to 1,030 °C with a flow of Ar (400 sccm) and H_2 (137 sccm) and anneal the foil for 4 h. The total base pressure during annealing is approximately 26 torr, maintained throughout steps 3–6 below.
(3) Increase the temperature to 1,040 °C.
(4) Flow 1% CH_4 diluted in H_2 (3 sccm), Ar (400 sccm) and H_2 (137 sccm) for 1 h.
(5) Cool to 600 °C at a cooling rate of 50 °C min in a flow of 1% CH_4 diluted in H_2 (3 sccm), Ar (400 sccm) and H_2 (137 sccm).
(6) Cool to room temperature in a flow of Ar (400 sccm) and H_2 (137 sccm).

Layer-by-layer stacking with interlayer rotational angle control. Our stacking method with aligned graphene building blocks provides reliable θ control. Supplementary Fig. 2 depicts the detailed procedures, where the blue arrows represent the crystalline orientation of graphene.

(1) Spin 8% 950 K PMMA in anisole on a graphene/copper surface at 1,000 rpm for 1 min.
(2) Bake it at 145 °C for 1 min.
(3) Attach thermal release tape with many 1 cm wide holes on a graphene/copper surface.
(4) Cut the thermal release tape into many pieces. Each piece of the tape has one hole.
(5) Etch the foil by floating the pieces on the surface of a diluted ammonia persulfate solution. (Volume ratio between saturated ammonia persulfate solution and water = 1:5)
(6) Move them to the surface of pure water after etching. Leave them on the surface for 5 min.
(7) Pick them up and blow dry the bottom surfaces with nitrogen.
(8) Transfer one piece onto a target substrate and drop a little bit of water at the interface.
(9) Bake it at 90 °C for 5 min to produce good adhesion with the target substrate.
(10) Activate the thermal release tape by heating it briefly at 115~140 °C.
(11) Lift off PMMA with acetone at 90 °C for 5 min and rinse the substrate with IPA.
(12) Anneal it in air at 350 °C for 15 min.
(13) Repeat the process from steps 8–12 to stack multiple layers of graphene. The controlled θ_{stack} is defined by the relative angle between the edges of the first and second pieces of transferred thermal release tape.

CD measurement. The CD effects are observed by measuring the absorption difference between the two circularly polarized light (I_L and I_R) perpendicularly through our samples. We use an Aviv 400 CD spectrometer, where lock-in measurements are conducted with circularly polarized light alternately switched from left-handed light to right-handed light with a frequency of 50 kHz. The light energy ranges from 2.0 eV to 5.5 eV with spectral bandwidth of 1 nm and a spot size at the sample of 5 mm × 1 mm.